CrossMark

Earth pressure evolution of the double-row long-short stabilizing pile system

Yongjiang Shen[1] · Yang Yu[2] · Fei Ma[1] · Feilong Mi[1] · Zhengliang Xiang[1]

Abstract Double-row stabilizing piles provide larger stabilizing force and lateral stiffness than the single ones. However, the loading shared by the front and rear pile is not the same with each other because of the shadow effects. A double-row long-short stabilizing pile system is verified in this paper. Physical model tests are used to investigate the influence of short rear pile on the earth pressures evolution in the stabilized soil. Numerical models are established and calibrated with the applied displacement–force curve and monitored earth pressure in the physical model test. The influence of the short rear stabilizing pile on the soil–pile interaction is further investigated based on the numerical model. The soil–pile relative displacement, total stabilizing force and bearing proportion of front and rear stabilizing pile are used to evaluate the soil–pile interaction. It is concluded that the total stabilizing force and bearing proportion of front and rear stabilizing pile are not significantly influence by the short rear stabilizing pile when the double-row piles are arranged in a line. When the double-row piles are arranged in a zigzag form, the total resistance provided by the double-row stabilizing piles decreases as the short rear piles are being used.

Keywords Pile–soil interaction · Double-row piles · Physical model test · Numerical simulation

✉ Yang Yu
   yang-yu@zju.edu.cn

1   School of Civil Engineering, Central South University, Changsha 410075, China

2   Ocean College, Zhejiang University, Zhoushan 316021, China

Introduction

How to control landslides is an attractive subject in the field of geotechnical and geological engineering. The stabilizing pile is one of the effective measurements that can solve such a problem. As the mountain areas are being explored, more and more potential large-scale landslides need to be stabilized. In such a situation, single-row stabilizing piles cannot provide enough stabilizing force in many cases. Various kinds of double-row stabilizing pile are being used to control large-scale landslides in practice. Although the double-row stabilizing piles are effective for the large-scale landslides, the construction budget and complexity will also increase by times (Xiao et al. 2017). On the other hand, the rear stabilizing piles will decrease the soil displacement around the front stabilizing piles and decrease the interaction between the soil and front stabilizing piles. This is called shadow effect, which will result that the front and rear stabilizing piles in lateral spreading soil cannot provide the same stabilizing force (Kourkoulis et al. 2011). In the view of construction convenient, the same size of cross section is used for the front and rear stabilizing piles in practice, which means they have the same bearing capacity. In such a situation, progressive failure of the pile system may happen due to the unbalanced distribution of the stabilizing force in the piles, which has been reported in engineering practice (Li et al. 2013a). As a result, how to balance the bending, shear and deformation between the front and rear stabilizing piles becomes an attracting subject both in theoretical and practical fields.

The bending, shearing and deforming behaviour of the front and rear stabilizing piles are related to the soil characteristics and pile arrangement. The limiting force and pile–soil interaction are mainly related to the soil characteristics. Among the others, Ito (1975) established

Springer

the model to calculate lateral force acting on piles based on plastic theory. Guo (2006) obtained the pile response under the action of lateral soil movement assuming that the pile–soil interaction with nonlinear springs, they found the soil modulus and pile–soil relative stiffness had significant impact on the pile response. Tang et al. (2014) obtained the evolution of earth pressure distributions along the stabilizing piles at different deformation stages of the sliding mass. Except for the parameters related to geotechnical material, researchers have done a lot of work to study the influence of centre-to-centre distance, row distance, embedded length, plain arrangement of the double-row piles and the connecting beam on the response of double-row stabilizing piles (Kahyaoglu et al. 2012; Li et al. 2013b; Yu et al. 2013). According to these researches, the cost-efficient centre-to-centre distance and row distance are 4–6 times and 4 times of pile diameter. Load sharing between double-row piles is more reasonable in the zigzag arrangement than in a parallel arrangement. Besides these factors, the construction time delay also increases the unbalance load sharing between double-row pile (Yu et al. 2012). The zigzag plane arrangement and connecting beam on the pile head can reduce shadow effects in some extent (Kourkoulis et al. 2011, 2012), but will increase the construction complexity and budget.

In this paper, we conduct physical model tests on full-length double-row piles and double-row long-short piles in order to investigate the earth pressure evolution and the difference of bearing capacity between these two pile systems. The earth pressures in the stabilized soil are monitored in order to analyse the evolution and range of soil arching. Numerical model is established using FLAC3D and calibrated with the monitored applied boundary displacement–force curve and earth pressures. The soil–pile relative displacement, total stabilizing force and bearing proportion are used to evaluate the influence of the short rear stabilizing piles. The influence of shear strength of soil close to the surface of sliding mass and the arrangement of double row on the bearing capacity of double-row long-short piles are also investigated.

Physical model test

The model size and materials

The framework of the model box is made of steels. The base panel, side panels and webs are all made of wood, which are fixed on the steel framework. Two steel boxes are placed in the middle part of the box below the base panel, as shown in Fig. 1. The front and rear stabilizing piles are embedded in the box with crushed rocks. The box is 1900 mm in length and 480 mm in width. The depth of
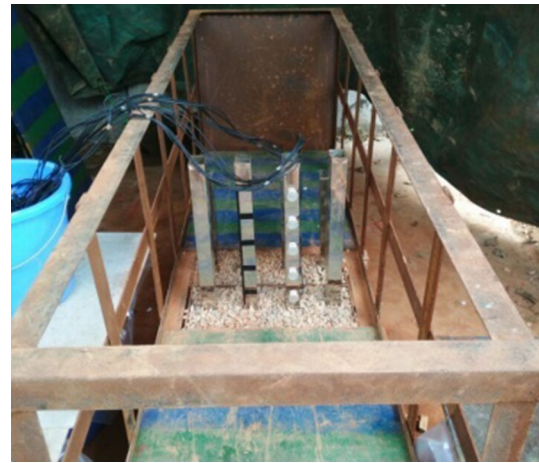

Fig. 1 The model box

the boxes used to embed the stabilizing piles is 200 mm. The depth of the landslide mass is 400 mm.

Rectangular aluminium pipe piles (40 mm × 60 mm) with 1.2 mm wall thickness are adopted as stabilizing piles. The length of the front pile is 600 mm with 400 mm in the sliding mass, which is a full-length pile. The length of the rear pile is 400 mm with 200 mm in the sliding mass, which is a short rear pile.

The sliding layer is composed of clay with the density of 1900 kg/m³. The undrained cohesion of the disturbed clay sample is 20 kPa, which is measured using the direct shear test. The friction angle of the clay is 0. Crushed rocks are used to fix the pile in the lower boxes, as shown in Fig. 2.

Loading and monitoring system

A mechanical jack with 30 kN maximum thrust force is adopted as the loading system. A mechanical sensor with maximum range 20 kN is used to measure the thrust force applied by the jack. The applied boundary displacement is obtained by measuring the elongation of the jack at each loading step. The jack, sensor and their installation are shown in Fig. 3.

Eighteen earth pressure cells combined with the data collector are used to measure the earth pressure variations during the loading steps. Eighteen earth pressure cells are installed in two vertical positions. The first vertical position is located at 100 mm above the sliding surface. The second vertical position is located at 300 mm above the sliding surface. Each vertical position has 9 earth pressure cells. The horizontal distance between each earth pressure cell is 60 mm. The coordinate and position of the earth pressure cells are shown in Fig. 4. Because the earth pressure cell can measure the earth pressure in one direction at each time, two tests are conducted for each of the full-length pile scenario and the full-length front pile and short rear pile

Fig. 2 Soil and rock materials. **a** Clay. **b** Crushed rock
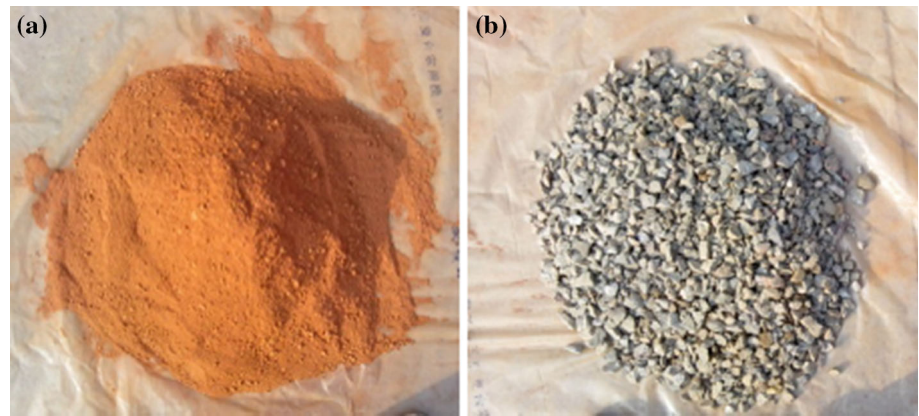

Fig. 3 Loading system

scenario. The test scenarios are summarized in Table 1. The earth pressure cells are firstly installed to measure the earth pressure parallel to the loading direction in one test (y direction) and then to measure the earth pressure perpendicular to the loading direction (x direction) in another test. A ruler with the accurate position of each cell is made and used to install the earth pressure cells in order to ensure the same position of each cell in different test scenarios. The installation of the cells is shown in Fig. 5.

Test procedures

The following procedures are repeated for each scenario of the four tests:

- The piles are inserted into the boxes. The crushed rocks are filled in the space between the boxes and piles in order to fix the piles.
- The earth pressure cells are installed.
- Plastic films are installed around the model box to reduce the friction between the slope and the model box. The clay is filled into the box layer by layer. Each layer is 100 mm in thickness. The layers are fully compacted using a 5-kg-weight hammer.
- The mechanical jack and the pressure sensor are installed at back side of the sliding layer. The pressure sensor is connected to the pressure display system.

- The initial data of earth pressure cells and the pressure sensors are set to be zero. The applied force is divided into six steps. A 1.2 kN increment is loaded in each step. After 15 min, the monitored data are recorded, and the next loading step is applied.

Test results

The rear pile are full-length piles

Figures 6 and 7 show the earth pressure variations under the loading of 3.6, 4.8, 6.0 and 7.2 kN. Figure 6 shows the earth pressure variations at position of $z = 100$ mm. It can be seen that the soil arching is mainly developed behind the rear stabilizing pile. Both the earth pressures in the x and y directions have a peak in the range of 240–420 mm, just behind the rear stabilizing pile. Such a range does not change as the loading increases. As the loading increases from 3.6 to 7.2 kN, the peak earth pressure increases from 4 to 16 kPa in the x direction and 30 to 90 kPa in the y direction, respectively. The position of the peak earth pressures in the x and y directions is constant at 300 mm. Both the earth pressures in the x and y directions between the front and rear piles are smaller than that behind the rear piles, which shows significant shadow effect.

Figure 7 shows the earth pressure variations at $z = 300$ mm. As shown in Fig. 7a, the earth pressure variation in the x direction is not larger than 4.0 kPa. As the loading increases from 3.6 to 4.8 kN, the earth pressure in the x direction increases. However, as the loading increases from 4.8 to 7.2 kN, the earth pressure in the x direction does not monotonically increase. The drifts and variations of the positions of the earth pressure cells due to soil uplifts and cracks initiation may be the main reasons for this phenomenon. As the loading increases, the soil behind the rear stabilizing pile will uplift and crack, which can lead to the relative displacement between soil and earth pressure cells. The interaction between the soil and the earth pressure cells
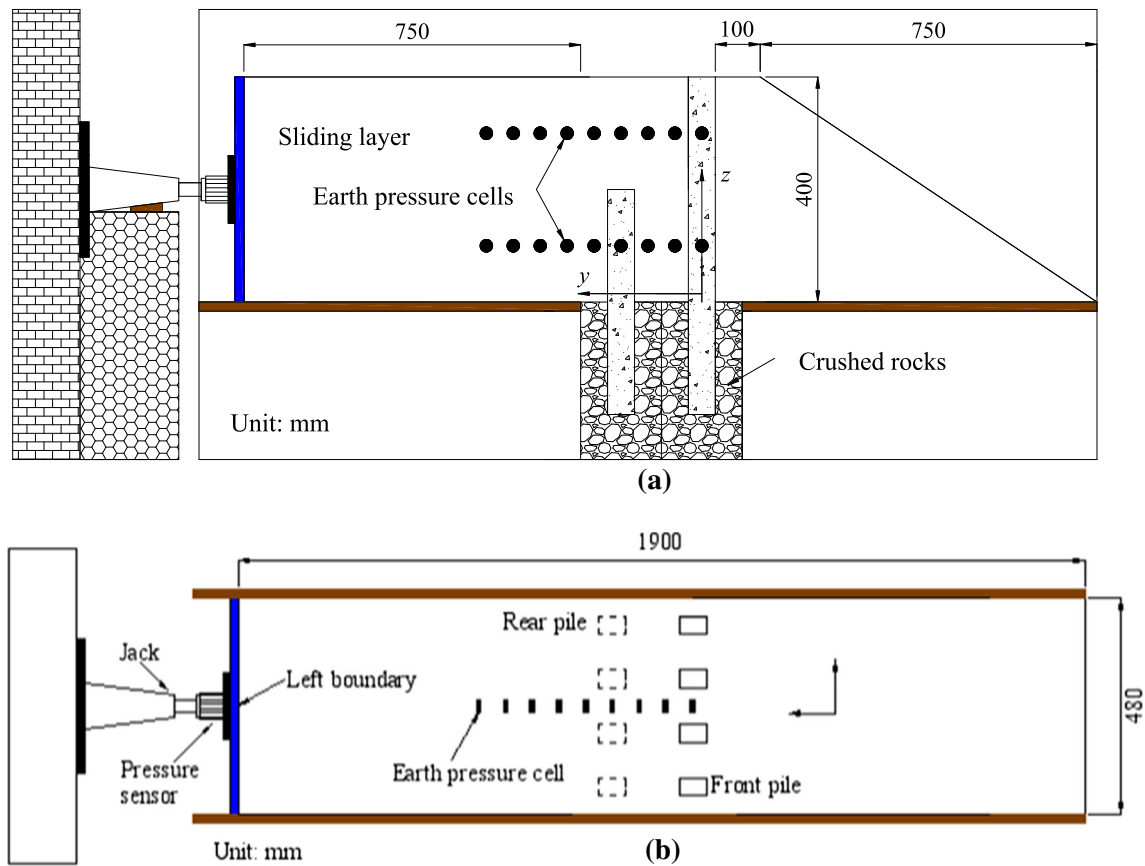
(a)

(b)

Fig. 4 Schematic show of the model and earth pressure cells. **a** Vertical view. **b** Top view

Table 1 Test scenarios

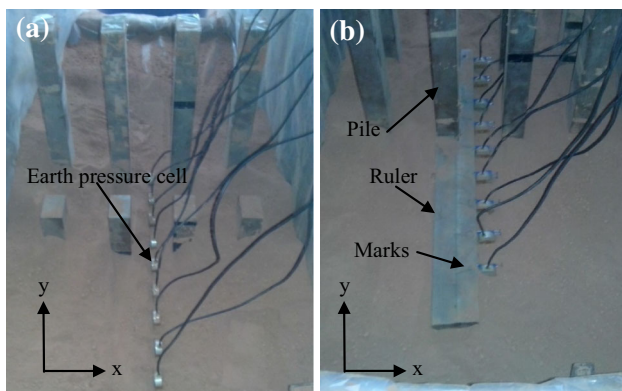| Test scenarios	No. 1	No. 2	No. 3	No. 4
Pile arrangement	Full-length front and rear stabilizing piles	Full-length front and rear stabilizing piles	Full-length front pile, short rear pile	Full-length front pile, short rear pile
Direction of monitored earth pressure	x	y	x	y

Fig. 5 The installation of earth pressure cells, **a** in x direction and **b** in y direction

will change, so do the monitored stresses. The drifts of the earth pressures will also influence the monitoring results. Although these factors only influence the monitored stresses in a small extent, the maximum magnitude of the earth pressure at $z = 300$ mm is much smaller than that at $z = 100$ mm, which leads to more sensitive variations of the monitored stresses at $z = 300$ mm than that at $z = 100$ mm. Figure 7b shows the earth pressure in the y direction increases as the loading increases. Soil arching develops behind the rear piles. No significant soil arching is observed between the front and rear piles.

Comparing the magnitudes of earth pressures between Figs. 6 and 7, it can be found that the earth pressures at $z = 100$ mm are much larger than that at $z = 300$ mm.
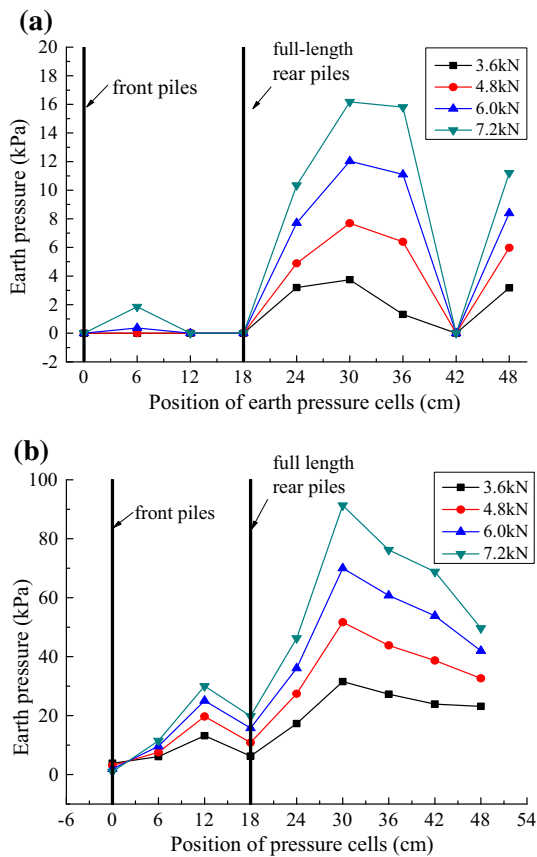
Fig. 6 Earth pressure variations at $z = 10$ cm (the rear stabilizing piles are full-length piles), **a** in x direction and **b** in y direction

Fig. 7 Earth pressure variations at $z = 30$ cm (the rear stabilizing piles are full-length piles), **a** in x direction and **b** in y direction

The reason for this phenomenon is not only attributed to different depths of these earth pressure cells, but also determined by the pile–soil interaction. The earth pressure acting on the piles and in the soil arches is determined by the relative displacement between the piles and the sliding soils (Cai and Ugai 2011). The piles can be considered as cantilever structures as the pile tops are free. When the uniform displacement is applied on the boundary of the sliding soil by the loading system, soil–pile relative displacement will occur. For the cantilever piles, the lateral displacement of the pile increases from the sliding surface to the top of the pile. As a result, the relative displacement between the soil and piles also increases from the sliding surface to the top of the piles. This leads to the earth pressure at $z = 300$ mm being smaller than that at $z = 100$ mm according to the subgrade reaction method, in which the lateral loading acting on the piles is proportional to the soil–pile relative displacement (Cai and Ugai 2011).

The rear pile is short piles

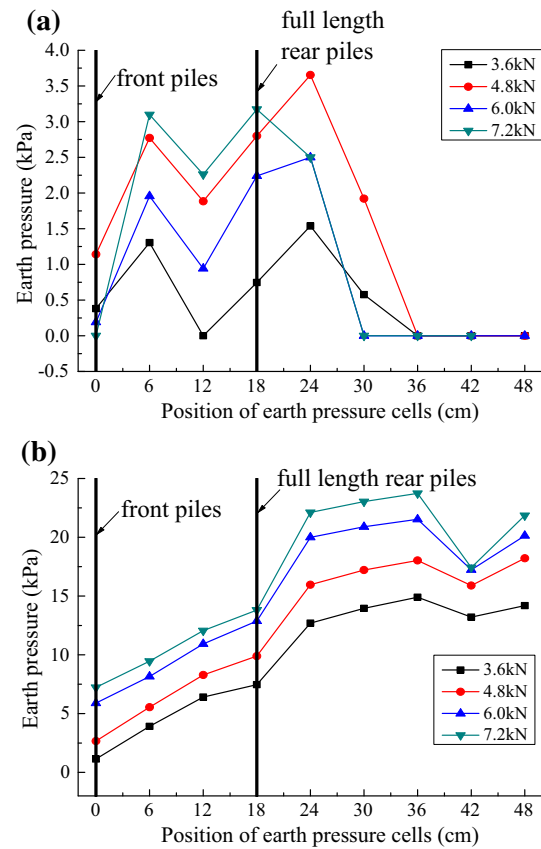Figures 8 and 9 show the monitored earth pressure variations when the rear stabilizing piles are 200 mm in the sliding layer. It can be seen in Fig. 8 that the soil arching is developed behind the rear stabilizing piles. The peak earth pressure in the x direction increases from 7 to 26 kPa as the loading increases from 3.6 to 7.2 kN. The peak earth pressure in the y direction is not as significant as the loading smaller than 4.8 kN. Soil arching is not developed in the soil between the front and rear stabilizing piles. Figure 8a shows that the earth pressures are larger at $x = 0$ than that at $x = 60$ mm and $x = 120$ mm, which illustrates the soil squeezes between the front piles. As a result, the earth pressures in the x direction increase, but keep constant in the y direction at the position of $x = 0$. In Fig. 8b, the earth pressure along the y direction decreases from the rear stabilizing pile to the front stabilizing pile, which means the soil between the front and rear stabilizing piles is squeezed by the rear stabilizing pile, and the deformation of the soil is not large enough to form soil arching between the front stabilizing piles.

Figure 9 shows earth pressure variations in the x and y directions at $z = 300$ mm, which is 100 mm higher than the top of the rear stabilizing piles. The earth pressure in the x direction only increases in the range of 0–60 mm as the loading increases. However, the earth pressure variation is smaller than 1.2 kPa. The maximum earth pressure
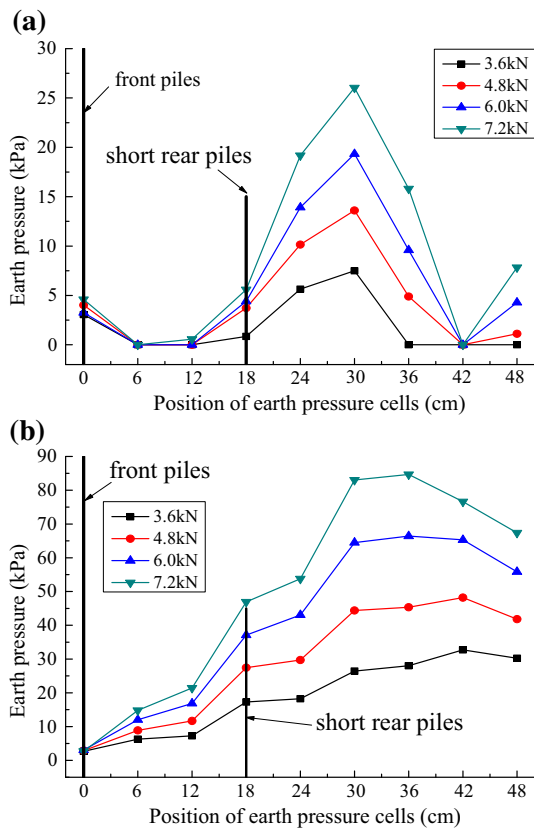
Fig. 8 Earth pressure variations at $z = 10$ cm (the rear stabilizing piles are short piles), **a** in x direction and **b** in y direction

Fig. 9 Earth pressure variations at $z = 30$ cm (the rear stabilizing piles are short piles), **a** in x direction and **b** in y direction

in the y direction is observed at the position close to the loading boundary. Although a peak earth pressure is observed at $x = 240$ mm, it can be concluded that no soil arching is developed because of the 0 earth pressures in the x directions, as shown in Fig. 9a. The 0 earth pressures may be attributed to that the earth pressure variation is smaller than the sensitivity of the earth pressure cells.

Numerical integration

Model calibration

Numerical models with the short rear stabilizing piles are established using FLAC3D in order to interpret the results of physical model tests. Due to the symmetry, half of the pile and soil between the piles are modelled in the numerical simulation. As a result, the width of the model is 60 mm. The length and depth of the sliding soil are the same as that of the physical model test, which is 1900 and 400 mm, respectively. The lengths of the front and rear stabilizing pile are 600 and 400 mm, respectively. Both embedded length of the front and rear stabilizing piles are 200 mm. The numerical model is shown in Fig. 10.
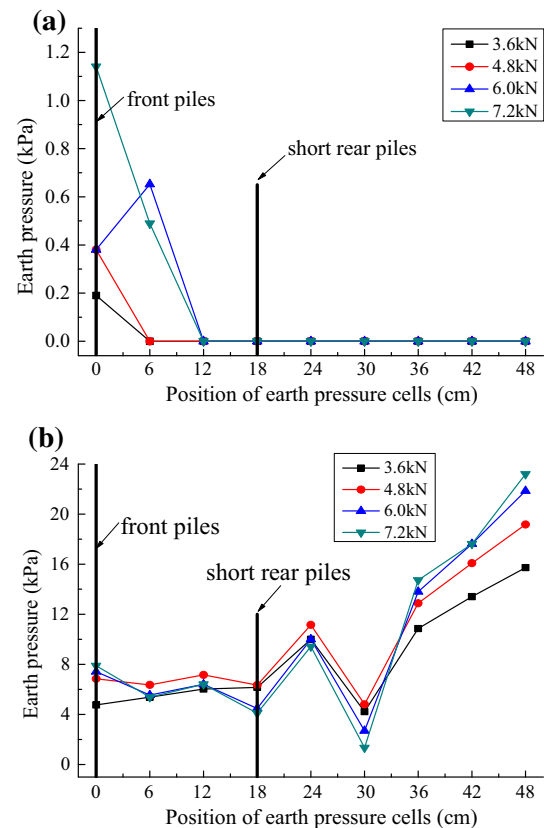
The crushed rocks and the stabilizing pile are modelled as linear elastic material. Rectangular pipe pile is used in the physical model test, while rectangular pile is used in the numerical simulation. The elastic modulus of the stabilizing pile is calculated according to the equality of the flexural rigidity of the two kinds of the piles. The density is calculated according to the equal weight of the hollow rectangular and rectangular piles. The Mohr–Coulomb failure criterion is used to model the sliding soil. The elastic modulus of the sliding soil is depth related, which is expressed as (ITASCA Consulting Group, Inc. 2005)

$$E = E_0 + a\sqrt{D} \tag{1}$$

where E_0 is the elastic modulus at the surface of the soil, D is the depth from the soil surface and a is a constant.

Because the soil is filled in the box layer by layer and is fully compacted using a 5-kg-weight hammer, we assumed that the cohesion of the soil is also depth related, which is expressed as

$$c = c_0 + bD \tag{2}$$

where c_0 is the cohesion at the surface of the soil, D is the depth from the soil surface and b is a constant.
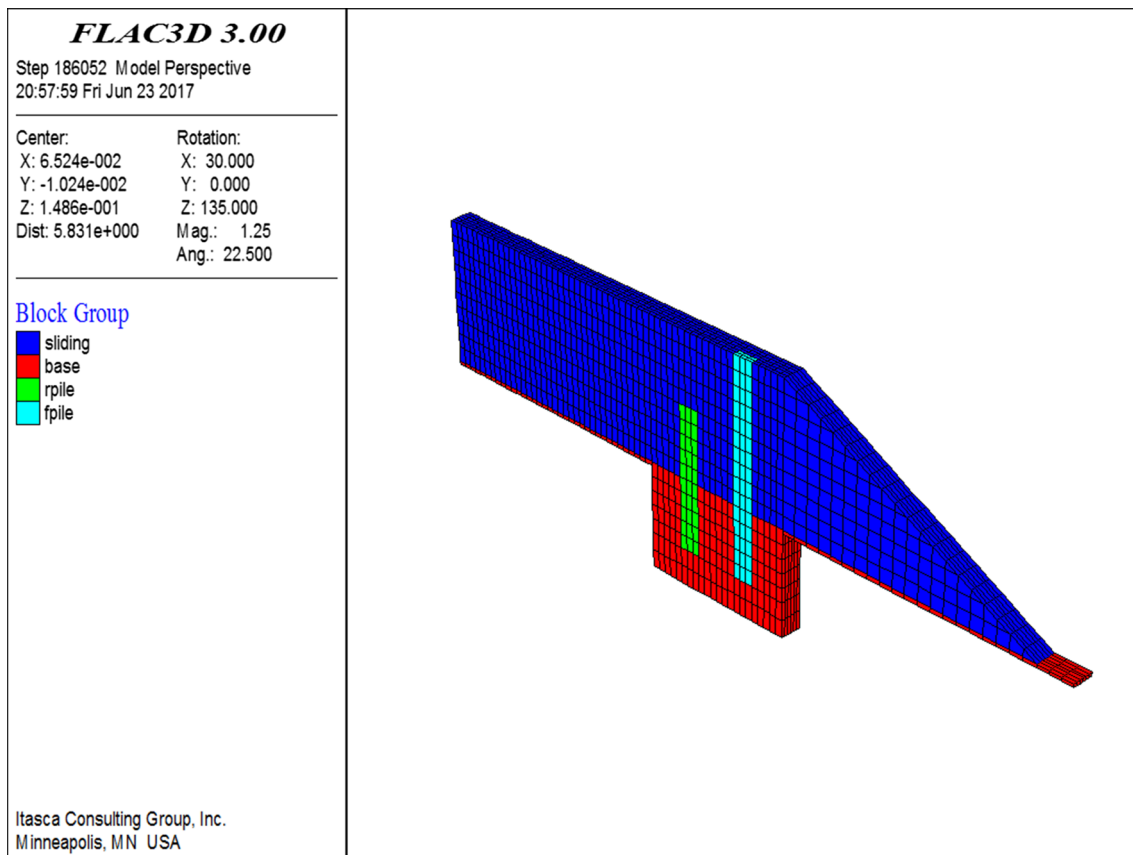
Fig. 10 The meshes of numerical model

The displacement on the symmetric plane is constrained. The displacement in x direction is constrained on the left and right boundary. The displacements of the base of the box are constrained in all the directions. Interfaces are established to model the pile–soil and base–soil contacts. The parameters of the interfaces are chosen according to the recommendation in the manual of the FLAC3D (ITASCA Consulting Group, Inc. 2005), which is expressed as

$$k_{\mathrm{n}} = k_{\mathrm{s}} = 10 \max \left(\frac{K + \frac{4}{3}G}{\Delta z} \right) \qquad (3)$$

where k_{n} is the normal rigidity of the interface, k_{s} is the shear rigidity of the interface, K and G are the bulk and shear of the material connecting to the interfaces and Δz is the minimum size of the element connecting to the interfaces.

The simulation is realized by applying initial velocity on the grid point of the left boundary of the sliding soil. The velocity is set as 0.5×10^{-4} mm per step in order to avoid large unbalance force. All the unknown constants are determined by fitting the numerical results with the physical model testing results.

The applied force–displacement curve and soil pressure monitored in the physical model test are used to calibrate the numerical model. The displacement and unbalanced force on the left boundary of the sliding mass are monitored during the simulation. As a result, the applied force–displacement curve of the numerical model can be obtained. The zone stress at the same position with the physical model tests is compared with the monitored stresses along x and y directions. Figure 11 shows the comparison between the measured and simulated applied force–displacement. When a good agreement is obtained at the loading of 3.6 kN, the coefficients in Eqs. (1) and (2) are determined. They will be used to predict the earth pressures in the next steps.

Figure 12 shows the comparison between the measured and simulated stresses. At the position of $z = 100$ mm, the numerical model captures the main characteristics of the stress in the x and y directions, such as the distribution shape and the peak value along the monitoring line. At the position of $z = 300$ mm, however, the distribution shape along the monitoring line is not captured accurately by the numerical model. The reason for this phenomenon is that uplifts and cracks are initiated in the soil closed to the
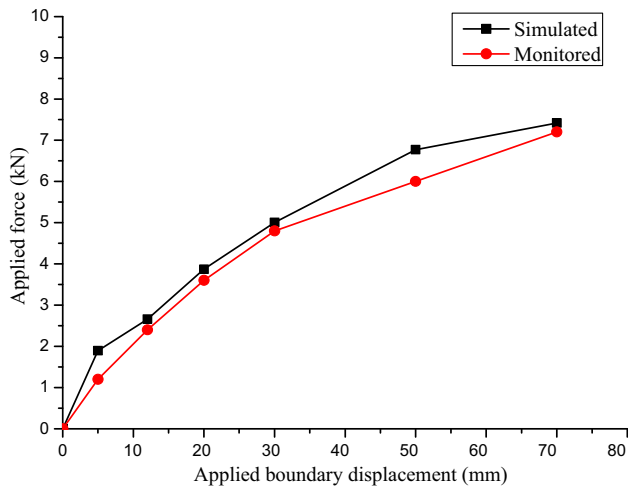
Fig. 11 Comparison between monitored and simulated applied force–displacement curves

surface as the loading increases. A sliding wedge will develop in the soil as the loading increases. A sliding surface will initiate from the bottom of the loading boundary to the soil surface behind the rear stabilizing pile. The uplifts and cracks will concentrate around the intersection of the sliding surface and the soil surface. The earth pressures before the sliding surface will decrease due to the soil uplifts and cracks initiation. The earth pressures behind the sliding surface will increase as the monitor points close to the loading boundary. Relative displacements between the earth pressure cells and the around soil may occur due to the soil uplifts and cracks initiation. This will also lead to the variations of the monitored earth pressures especially at $z = 100$ mm, where the maximum magnitude of earth pressure is only 4 kPa. As a result, the earth pressure cells will be more sensitive to the soil uplifts and cracks initiation at $z = 300$ mm than that at $z = 100$ mm. In the
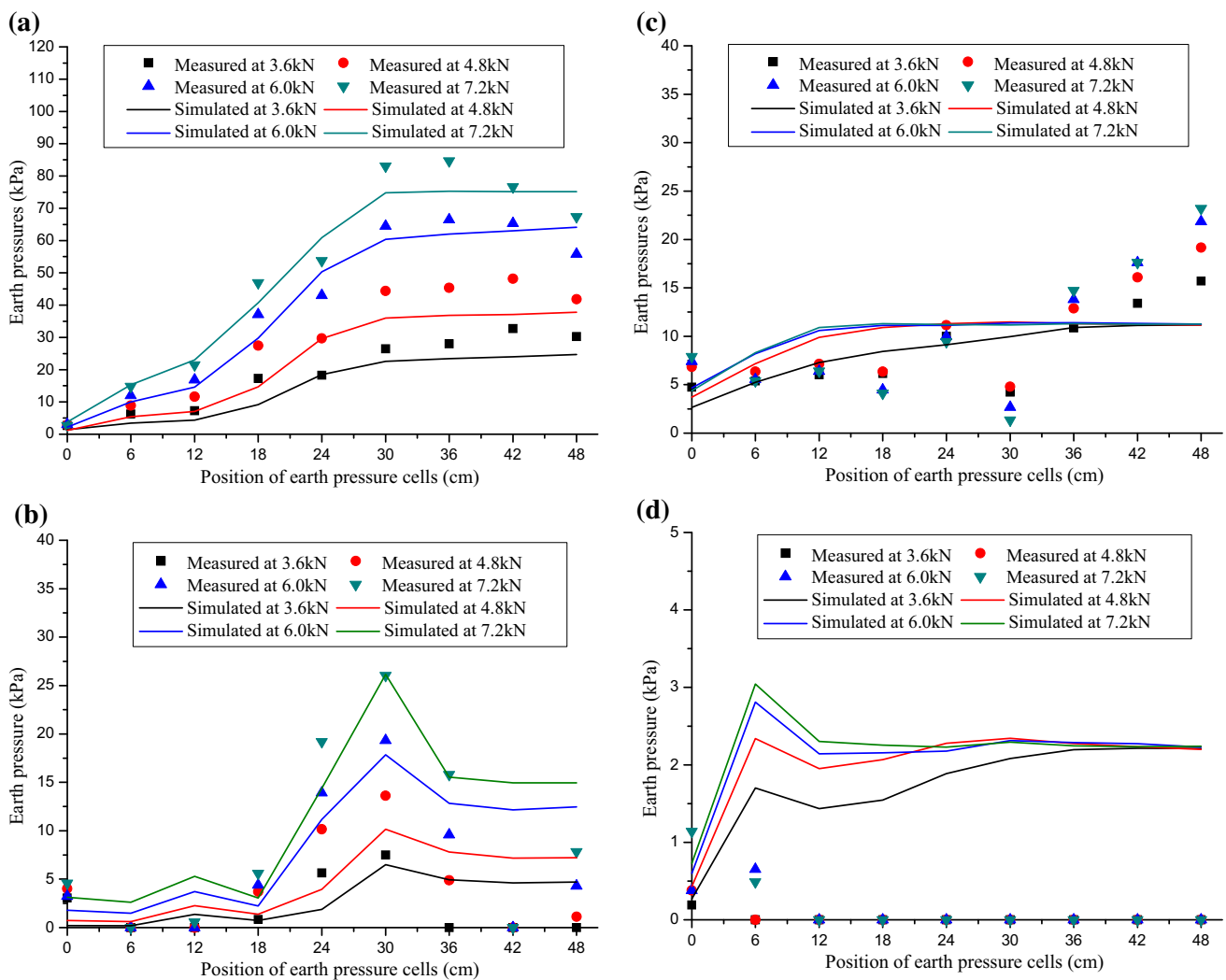

Fig. 12 Comparison between monitored and simulated earth pressures, **a** in x direction at $z = 10$ cm, **b** in y direction at $z = 10$ cm, **c** in x direction at $z = 30$ cm and **d** in y direction at $z = 30$ cm

Table 2 Soil parameters in numerical simulation

Material	Model	E (kPa)	v	Cohesion (kPa)	Friction angle (degree)	Density (kg/m^3)
Sliding soil	Mohr–Coulomb	$0.5 + 50 \sqrt{D}$	0.2	$5 + 16D$	0	1820
Rock and the tank base	Elastic	5.2×10^5	0.2	–	–	1900
Pile	Elastic	5.81×10^6	0.32	–	–	260

Table 3 Interface parameters in numerical simulation

Interface	k_n (GP)	k_s (GPa)	Cohesion (kPa)
Soil–pile	8.313	8.313	10
Soil–base	2.892	2.892	10

numerical model, such a phenomenon cannot be modelled appropriately. In the physical model, as the loading increases, the soil close to the loading boundary will increase in density, so do the shear strength and elastic modulus. However, these parameter variations are difficult to be obtained in the physical model. As a result, we cannot simulate this process as the soil parameters are assumed to be constant in the numerical model.

As the earth pressure variation between different loading steps measured in the tests is very small, which means the soil in the monitored region has been in plastic state since the loading equal to 3.6 kN. This phenomenon is captured by the numerical model. As a result, we believe the numerical model can help us to study the soil arching development in the physical model tests. The calibrated soil parameters and interface parameters are shown in Tables 2 and 3, respectively.

Soil arching in vertical direction

The soil–pile relative displacement is equal to the soil displacement in the central of the two piles minus the pile displacement. No matter in the elastic foundation beam or p–y curve method, the earth pressure acting on the piles is proportional to the soil–pile relative displacement. Larger soil–pile relative displacement means larger earth pressures acting on the pile. The stability and strength of soil arching are not only related to the soil mechanical parameters such as the friction angle and cohesion, but also related to the earth pressure at the foots of soil arching. Larger earth pressure means larger bearing capacity of the soil arching.

Figure 13 shows the soil–pile relative displacements under different boundary displacements when the rear stabilizing pile is full length (400 mm in the sliding layer) and 200 mm in the sliding layer. The relative displacement of the short rear pile scenario is smaller that of the full-length scenario in the region 200 mm above the sliding surface, while this situation is opposite in the region
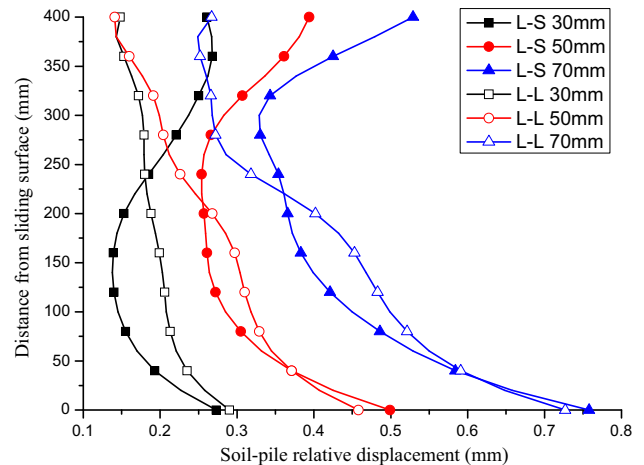

Fig. 13 Comparison of soil–pile relative displacements between L–L and L–S under applied boundary displacement of 30, 50 and 70 mm

200–400 mm from the sliding surface. This phenomenon illustrates that the soil arching effect decreases in the lower part but increases in the upper part of the front pile due to the rear pile being buried in the soil.

Influence of buried depth on the stabilizing force

Figure 14 shows the total shear force of the front and rear stabilizing piles in the section located at the sliding surface. The total shear force is equal to the stabilizing force of the landslide provided by the double-row piles. Two scenarios are considered in Fig. 14. The first scenario is both the front and rear stabilizing piles which are full-length piles in the sliding layer (legend L–L). The second scenario is the front stabilizing pile which is full-length pile, while the rear stabilizing piles are 200 mm short pile in the sliding layer (legend L–S).

It can be seen in Fig. 14 that the stabilizing force between the L–L and L–S is the same under the action of different applied boundary displacements. It illustrates that the short rear stabilizing pile does not lead to the reduction in stabilizing force. The reason for this phenomenon can be explained by the soil–pile relative displacement in Fig. 13. When the short rear stabilizing piles are used, the soil–pile relative displacement in the range of $z = 200$–400 mm increases, while above the soil–pile relative displacement in the range of $z = 0$ to $z = 200$ mm decreases. The
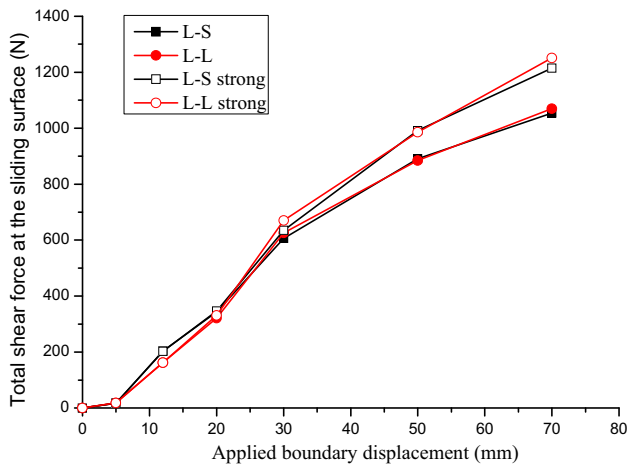
Fig. 14 Total resistance provided by double-row piles under different applied boundary displacements

absolute increment is larger than the absolute decrement. The elastic modulus and soil shear strength parameters of the numerical model increase over the depth. Smaller earth pressure is developed on the piles closed to the soil surface comparing with that close to the sliding surface due to the smaller coefficient of elastic foundation close to the soil surface. Although the soil–pile relative displacement increases close to the soil surface due to the short rear stabilizing pile, the earth pressure on the upper part of the piles does not increase since the soil with weak shear strength parameters has been in plastic state. In order to verify this point, we increase the cohesion close to the soil surface from 5 to 20 kPa (legend L–S strong and L–L strong) and maintain the other parameters as the original values. The stabilizing forces with strong soil shear strength parameters are larger than that with weak soil shear strength parameters comparing with corresponding pile scenarios when the applied boundary displacement is larger than 20 mm.

Figure 15 shows the proportion of stabilizing force provided by the front and rear stabilizing piles to the total stabilizing force. As the applied displacement increases, the bearing proportion of front and rear pile increases and decreases, respectively. When the applied displacement is smaller than 30 mm, the front pile in the L–S scenario bears lower thrust than that in the L–L scenario, while the rear pile in the L–S scenario bears higher thrust than that in the L–L scenario. The proportion variation is more significant when the applied displacement is smaller than 30 mm. When the applied displacement is larger than 30 mm, the bearing proportion in the L–L scenario is almost the same as that in the L–S scenario. As a result, the advantages of the L–S stabilizing piles are not obvious for sliding soil with large displacement.
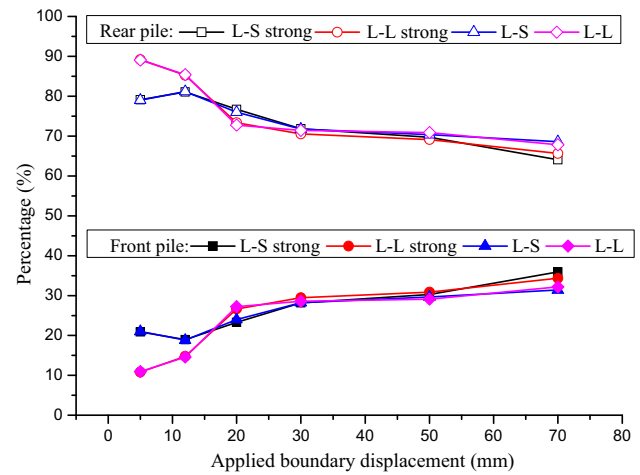

Fig. 15 Bearing proportions of the front and rear stabilizing pile under different soil shear strengths

Influence of pile arrangement

The physical model test and numerical simulation show that the shadow effects are not significantly weakened by the short rear piles when the front and rear piles are arranged in a parallel form. When the front and rear stabilizing piles are arranged in a zigzag form, the shadow effects can be weakened in some extent (Kourkoulis et al. 2012). In this section, zigzag arranged piles are used in the numerical model to investigate the influence of short rear stabilizing piles. Figure 16 shows the comparison of total resistance between the L–L and L–S scenarios. When the applied displacement is smaller than 20 mm, the short rear stabilizing pile has no influence on the total shear force in both the L–L and L–S scenarios. When the applied displacement is larger than 20 mm, the total shear force of the L–S scenario is lower than that of the L–L scenario. The zigzag arrangement form decreases the centre-to-centre
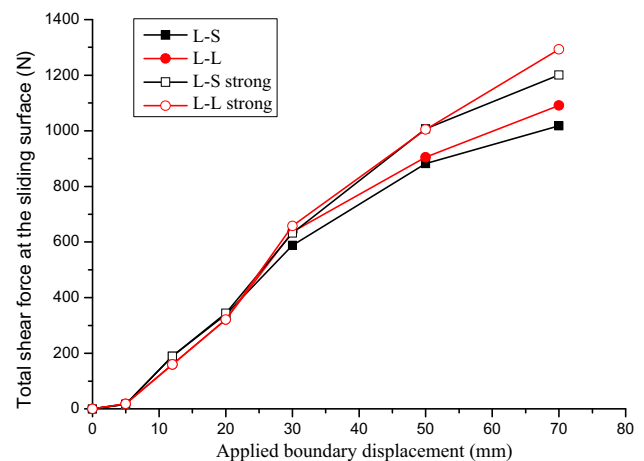

Fig. 16 Total resistance provided by double-row piles arranged in zigzag form

distance of the double-row stabilizing pile when the front and rear stabilizing piles are all full-length piles. As the rear stabilizing pile getting shorter, the original soil arching close to the soil surface will be destroyed. Consequently, the stabilizing force decreases as the centre-to-centre distance increases when the rear stabilizing pile getting shorter.

Conclusions

Based on the physical tests and numerical simulations, the following conclusions are obtained:

1. Both the earth pressures in the x and y directions show that the soil arching is more significant in the deep soil.

2. The long-short double-row stabilizing pile would be more suitable for soil with strong shear parameters. The short rear stabilizing pile increases the soil–pile relative displacement of the front stabilizing pile. More thrust will be transferred to the front pile if the shear strength of the soil is high enough.

3. It is found that the resistance provided by the double-row long-short stabilizing pile is the same as that provided by the full-length double-row stabilizing piles. This illustrates that the construction budget can be decreased without scarifying the resistance of the double-row stabilizing piles.

4. The zigzag arrangement form decreases the centre-to-centre distance of the double-row stabilizing pile when the front and rear stabilizing piles are all full-length piles, especially when the applied boundary displacement is larger than 20 mm. As the rear stabilizing pile getting shorter, the original soil arching close to the soil surface will not exist. Consequently, the stabilizing force decreases as the centre-to-centre distance increases when the short rear stabilizing pile is used. This phenomenon is different from the situation when the double-row piles are arranged in a parallel form.

References

Cai F, Ugai K (2011) A subgrade reaction solution for piles to stabilise landslides. Geotechnique 61:143–151. doi:10.1680/geot.9.P.026

Guo WD (2006) On limiting force profile, slip depth and response of lateral piles. Comput Geotech 33:47–67. doi:10.1016/j.compgeo.2006.02.001

ITASCA Consulting Group, Inc. (2005) FLAC3D (Fast Lagrangian analysis of continua in three dimensions) version 3.0, user's guide. ITASCA Consulting Group, Inc., Minneapolis

Ito T (1975) Methods to estimate lateral force acting on stabilizing piles. Soils Found 15:43–59

Kahyaoglu MR, Imancli G, Onal O, Kayalar AS (2012) Numerical analyses of piles subjected to lateral soil movement. KSCE J Civ Eng 16:562–570. doi:10.1007/s12205-012-1354-6

Kourkoulis R, Gelagoti F, Anastasopoulos I, Gazetas G (2011) Slope stabilizing piles and pile-groups: parametric study and design insights. J Geotech Geoenviron 137:663–677. doi:10.1061/(Asce)Gt.1943-5606.0000479

Kourkoulis R, Gelagoti F, Anastasopoulos I, Gazetas G (2012) Hybrid method for analysis and design of slope stabilizing piles. J Geotech Geoenviron 138:1–14. doi:10.1061/(Asce)Gt.1943-5606.0000546

Li TB, Tian XL, Han WX, Ren Y, He Y, Wei YX (2013a) Centrifugal model tests on sliding failure of a pile-stabilized high fill slope. Rock Soil Mech 34:3061–3070 **(in Chinese)**

Li CD, Tang HM, Hu XL, Wang LQ (2013b) Numerical modelling study of the load sharing law of anti-sliding piles based on the soil arching effect for Erliban landslide, China. KSCE J Civ Eng 17:1251–1262. doi:10.1007/s12205-013-0074-x

Tang HM, Hu XL, Xu C, Li CD, Yong R, Wang LQ (2014) A novel approach for determining landslide pushing force based on landslide-pile interactions. Eng Geol 182:15–24. doi:10.1016/j.enggeo.2014.07.024

Xiao S, Zeng J, Yan Y (2017) A rational layout of double-row stabilizing piles for large-scale landslide control. Bull Eng Geol Environ 76(1):309–321

Yu Y, Shang YQ, Sun HY (2012) Bending behavior of double-row stabilizing piles with constructional time delay. J Zhejiang Univ Sci A 13:596–609. doi:10.1631/jzus.A1200027

Yu Y, Sun HY, Shang YQ (2013) Influence of anchorage depth on mechanical behaviour of double-row anti-slide piles. Chin J Rock Mech Eng 32:1999–2007 **(in Chinese)**